

A first-principles study on the lattice thermal conductivity of irradiated glassy states of the $\text{Ge}_2\text{Sb}_2\text{Te}_5$ phase-change memory material

Felix C. Mocanu,^{a)} Konstantinos Konstantinou, and Stephen R. Elliott

Department of Chemistry, University of Cambridge, Lensfield Road, CB2 1EW, Cambridge, United Kingdom

(Dated: 13 December 2021)

An analysis of thermal transients from non-equilibrium *ab initio* molecular-dynamics simulations can be used to calculate the thermal conductivity of materials with a short phonon mean-free path. We adapt the approach-to-equilibrium methodology to the three-dimensional case of a simulation that consists of a cubic core region at higher temperature approaching thermal equilibrium with a thermostatted boundary. This leads to estimates of the lattice thermal conductivity for the glassy state of the phase-change memory material, $\text{Ge}_2\text{Sb}_2\text{Te}_5$, which are close to previously reported experimental measurements. Self-atom irradiation of the material, modelled using thermal spikes and stochastic-boundary conditions, results in glassy models with a significant reduction of the lattice thermal conductivity compared to the pristine glassy structure. This approach may prove to be useful in technological applications, e.g. for the suppression of thermal cross-talk in phase-change memory and data-storage devices.

The cost of computation is significantly determined by the energy needed to keep key components cool, whether it is central processing units, accelerators, memory or data storage. Even when components are kept at reasonable temperatures during normal operation, there may still be thermal-throttling under peak-load which affects their performance and lifetime. Hence, the ability to predict the thermal properties of solids is critical for the rational design of materials and the management of devices that are sensitive to thermal fluctuations.^{1,2}

Phase-change memory devices, which are widely believed to be a part of at least some commercial non-volatile solid-state drives, rely on the fast and reversible switching between a conductive crystalline phase (the “1” state of a bit), and a resistive glassy phase (the “0” state of a bit), of the same chalcogenide material, induced via Joule heating from the application of appropriate voltage pulses.³ Consequently, thermal cross-talk between adjacent memory cells can limit the size down-scaling in phase-change memory devices.⁴ An understanding of the thermal-transport properties of these materials at the atomic level is therefore essential for their design and optimization.⁵

The lattice thermal conductivity of the phase-change memory material, GeTe , has been predicted successfully with quasi-static calculations,⁶ as well as with classical equilibrium,⁷ and non-equilibrium,^{7,8} molecular-dynamics methods by using a linear-scaling neural-network interatomic potential.⁶ First-principles calculations were also employed to estimate the thermal conductivity for the crystalline phases of different chalcogenide phase-change materials, including $\text{Ge}_2\text{Sb}_2\text{Te}_5$,⁹ in good agreement with experimental observations. However, there are no previously reported modelling studies of the lattice thermal conductivity for the glassy phase of

$\text{Ge}_2\text{Sb}_2\text{Te}_5$ which is of equal importance with the crystalline counterpart for technological applications.

Methods for simulating thermal transport at the atomic level have seen a rapid evolution and are getting closer to quantitative agreement with experimental measurements.^{8,10} *Ab initio* methods, based on the Boltzmann transport equation,^{11,12} or on Green-Kubo dynamical formulations,^{13,14} have been employed recently in the literature to provide a first-principles description of thermal transport, and they represent significant advances in the field. Nevertheless, these approaches are computationally very demanding within a density-functional-theory framework, while some of them are specifically designed for harmonic solids near equilibrium.

Therefore, there is the necessity for an efficient first-principles molecular-dynamics approach to model the thermal properties of glasses and in particular the glassy phase of $\text{Ge}_2\text{Sb}_2\text{Te}_5$. An efficient and quantitative assessment of lattice thermal conductivity can be obtained from the approach-to-equilibrium molecular-dynamics (AEMD) method,^{15,16} which has been successfully deployed in *ab initio* (as well as with empirical force fields) molecular-dynamics simulations of several different materials.¹⁷

In this Letter, the AEMD methodology, which belongs to a larger class of non-equilibrium molecular dynamics (NEMD) methods, has been adapted to the case of a cubic core region in contact with a thermostatted boundary shell in order to calculate the thermal conductivity of irradiated glassy $\text{Ge}_2\text{Sb}_2\text{Te}_5$. Below, we briefly describe the computational details of the NEMD simulation protocol using stochastic-boundary conditions that is used to simulate the energetic thermal spikes. Numerical results are presented, starting with the fitting of thermal transients, the predicted thermal conductivity and the effect of irradiation on the thermal properties. We also compare our findings to experimental data and previous simulation studies, and we discuss some of the limitations of the approach.

^{a)} fcm29@cam.ac.uk

The simulated system is a 315-atom melt-quenched model of glassy $\text{Ge}_2\text{Sb}_2\text{Te}_5$.¹⁸ The simulation box, which has a length of 21.65 Å, was divided into a core cubic region and an outer boundary shell of thickness 1 Å on each side. This type of separation has been dubbed stochastic-boundary conditions, and was originally used to investigate thermal transport at interfaces.¹⁹ The core region samples a micro-canonical ensemble (NVE) while the boundary undergoes Langevin dynamics in the canonical ensemble (NVT) and dissipates the heat generated in the core region, during an ionic cascade.²⁰ The thermostat parameters were chosen such that the damping period was 100 fs. *Ab initio* molecular-dynamics simulations were carried out using the CP2K code,²¹ in which the stochastic-boundary-conditions approach is implemented, based on the Generalized Langevin Equation formulation.²² We modelled radiation-induced non-equilibrium cascades by performing thermal-spike simulations with initial kinetic energies in the range of 15 – 200 eV. Further details related to the computational set-up, the radiation-damage cascades and the *ab initio* molecular-dynamics simulations can be found in our previous work,^{23,24} where some of the initial trajectories used in this work have been taken from.

In the approach-to-equilibrium methodology, heat conduction is usually modelled by Fourier’s law.¹⁶ Based on our set-up, the simulation box is cubic and is assumed to be approximately homogeneous and isotropic. Additionally, we have considered that the boundary region acts as a “thermal wall” at a temperature of T_0 (300 K) and the core region will rapidly come into equilibrium with it after the cascade. In practice, the temperature of the boundary region will oscillate significantly and there will be an artificial thermal boundary resistance at the interface with the core region due to the thermostat that is employed in the outer shell.^{19,25,26} The Cartesian coordinates of atoms in the core region, x , y and z , reside in the real interval $[0, L]$ where $L = a - 2r$, a is the size of the periodic cubic simulation box and r is the thickness of the boundary region. Under these assumptions, the resulting heat equation can be written as:

$$\frac{\partial T}{\partial t} = -\alpha \left(\frac{\partial^2 T}{\partial x^2} + \frac{\partial^2 T}{\partial y^2} + \frac{\partial^2 T}{\partial z^2} \right) \quad (1)$$

where T is the temperature and t is the time.

The thermal diffusivity α is defined as:

$$\alpha = \frac{\kappa}{C_v \rho} \quad (2)$$

where κ is the thermal conductivity, C_v the constant-volume heat capacity and ρ the density of the system. The general solution, assuming a separable form, is then

given by:

$$T(x, y, z, t) = T_0 + \sum_{n=1}^{\infty} \sum_{m=1}^{\infty} \sum_{l=1}^{\infty} a_{nml} e^{-\alpha \lambda_{nml} t} \sin\left(\frac{n\pi x}{L}\right) \sin\left(\frac{m\pi y}{L}\right) \sin\left(\frac{l\pi z}{L}\right) \quad (3)$$

The Fourier-series coefficients in the general solution, λ_{nml} and a_{nml} , can be inferred from the boundary conditions and are given in the two equations below:

$$\lambda_{nml} = \left(\frac{\pi}{L}\right)^2 (n^2 + m^2 + l^2) \quad (4)$$

$$a_{nml} = -\Delta T_0 \left(\frac{2}{\pi}\right)^3 \frac{(1 - (-1)^n)(1 - (-1)^m)(1 - (-1)^l)}{nml} \quad (5)$$

The difference between the spatially averaged temperature of the core region (undergoing NVE dynamics) and the target temperature of the thermostatted boundary region (undergoing Langevin NVT dynamics) corresponds to: $\Delta T(t) = T(t) - T_0$. It has an initial value, ΔT_0 , at the start of the thermal quench and it decays to zero during the quench.

$$\Delta T \sim e^{-\frac{t}{\tau}} \quad (6)$$

The exponential temporal decay of this temperature difference in equation 6, has a dominant contribution from the leading term $n = m = l = 1$ of the Fourier series in equation 3. Once the relaxation time τ is obtained from simulations, it can be inserted into the time-dependent part of this dominant term. Hence, the thermal conductivity, κ , can be calculated from the expression:

$$\kappa = \frac{L^2}{3\pi^2} \frac{C_v \rho}{\tau} \quad (7)$$

The thermal transients of the non-equilibrium ion-irradiation simulations for glassy $\text{Ge}_2\text{Sb}_2\text{Te}_5$ can be directly fitted from the thermal quench of the core region as it reaches thermal equilibrium with the boundary layer. The trajectory of the radiation-induced cascade can be split into three intervals, based on the time evolution of the kinetic temperature, shown in figure 1 for different initial thermal-spike kinetic energies: (a) The high-energy cascade generated by the thermal spike; (b) An approach-to-equilibrium transient that is reasonably well described by an exponential temporal decay of the temperature difference between the core and the boundary; and (c) An equilibrium region where the system as a whole fluctuates around the target temperature of the thermostatted boundary layer (300 K).

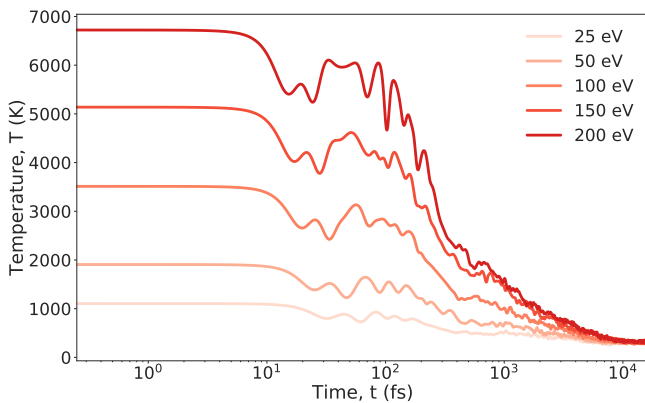


FIG. 1. Temperature (K) versus time (fs), on a linear-log graph, for a model of glassy $\text{Ge}_2\text{Sb}_2\text{Te}_5$, for different thermal-spike energies, shown as shades of red (darker means higher energy). The characteristic dips in temperature correspond to collision events during the non-equilibrium cascade. This is followed by an exponential decay of the temperature as the system approaches equilibrium, while at the end, the kinetic temperature of the system fluctuates around 300 K.

By examining the approach-to-equilibrium of the system after the high-energy cascade, thermal-conductivity estimates are obtained “on the fly” without having to run a separate simulation for this purpose. It is important to only fit the relaxation time τ using data from a restricted time interval in which the temperature decays exponentially. In practice this means including data only after the shock of the thermal spike has been absorbed by the boundary and just before reaching equilibrium. In order to avoid including data from the high-energy cascade at the beginning of the simulation, a time period of 1 – 2 ps from the start of the simulation needs to be removed from the fitting interval, based on the initial energy of the thermal spike, as indicated by our kinetic analysis of the approximate cascade duration.²⁴ Examples of exponential fits of the thermal relaxation time from the asymptotic regime of the ion-irradiation simulations are shown in figure 2 for 50 eV, 100 eV and 200 eV initial thermal-spike energies.

After obtaining the transients for all the thermal-spike simulations, we examined the thermal conductivity of the initial pristine glassy $\text{Ge}_2\text{Sb}_2\text{Te}_5$ structure. The computational procedure used in this case comprised the following steps: (1) Fix the atoms in the boundary region; (2) Initialize and equilibrate the velocities in the core region at a higher temperature; (3) Release the constraints for the boundary region; and (4) Remove the thermostat from the core region. In this case, there is no radiation-induced cascade and the simulation consists simply of a thermal quench and equilibration with the boundary. The core-region initial maximum kinetic temperature was chosen to be 700 K in order to avoid any intermixing between the core and the boundary.

The thermal relaxation times corresponding to the different ion-irradiation simulations and to the pristine

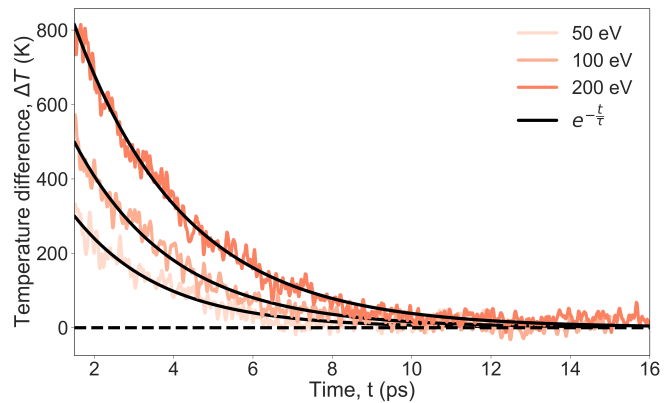


FIG. 2. The temperature difference ΔT between the core region and the target temperature of the boundary thermostat, viz. 300 K, as a function of time. Thermal transients in the approach-to-equilibrium are shown in different shades of red as a function of the energy of the thermal spike (darker is higher). The corresponding exponential fits are shown as black lines.

glassy $\text{Ge}_2\text{Sb}_2\text{Te}_5$ structure were calculated, and are shown in figure 3. It can be observed that the relaxation time τ scales as a power-law function of the initial energy of the thermal spike. The temperature evolution is regularly analyzed after simulations of thermal spikes and a mechanical model predicts that the thermal relaxation time will scale as a power-law function of the thermal-spike energy, with an exponent around $2/3$.²⁷ However, values for the power-law exponent below $2/3$ have been reported from computer simulations, suggesting that the exponent depends on the structure of the material.²⁸ From our simulations, a best-fit power-law exponent of 0.354 was obtained for glassy $\text{Ge}_2\text{Sb}_2\text{Te}_5$, indicating a gentle increase of the thermal relaxation time with the energy of the thermal spike. We expect that this trend will not be significantly changed if the calculation is repeated for several independent amorphous models or indeed a larger model to accommodate higher thermal-spike energies.

An additional ingredient for the estimation of the lattice thermal conductivity is the heat capacity of the material. In order to obtain the heat capacity, energy fluctuations, $\delta E = E - \langle E \rangle$, were sampled from equilibrium *ab initio* molecular-dynamics simulations. The starting point for each trajectory corresponds to the structural models at the end of each non-equilibrium thermal-spike simulation. In these subsequent molecular-dynamics runs, there is no longer a separation between core and boundary, and the entire system undergoes NVT dynamics with a single Langevin equation (GLE), or colored-noise, thermostat.^{29,30} Trajectories of 40 ps were generated with a time-step of 1 fs for each glassy sample. The first 8 ps were discarded and the heat capacity was estimated from the remaining 32000 time steps.

The calculated heat capacity at 300 K for the pristine glassy phase of $\text{Ge}_2\text{Sb}_2\text{Te}_5$ was $272 \pm 60.19 \text{ J kg}^{-1}$

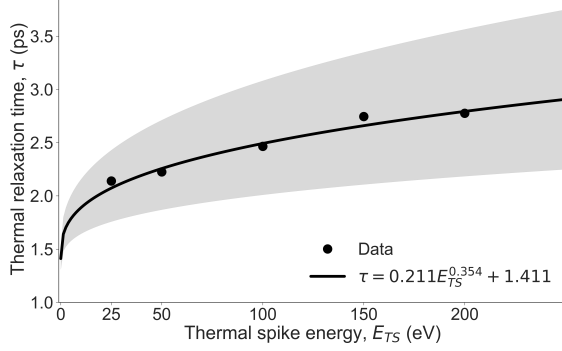


FIG. 3. Thermal relaxation times versus the initial kinetic energy of the thermal-spike atom. Data points are shown as black circles. A power-law fit to the ion-irradiation data is shown as the solid black line and the shaded region is the 95% confidence interval of the fit.

K^{-1} , which is above the Dulong-Petit limit value of $219 \text{ J kg}^{-1}\text{K}^{-1}$ ($3Nk_B$). This is in good agreement with experimental data from differential scanning calorimetry, viz. $220 - 230 \text{ J kg}^{-1} \text{ K}^{-1}$,^{31,32} and with the fact that the Debye temperature of glassy (as-deposited) $\text{Ge}_2\text{Sb}_2\text{Te}_5$ was found to be below 111 K from inelastic neutron-scattering experiments.³² In the Supplemental Material, details are provided for the calculation of the heat capacity and thermal conductivity in all of the simulated systems.

The lattice thermal conductivity of glassy $\text{Ge}_2\text{Sb}_2\text{Te}_5$ was calculated from equation 7, using a relaxation time corresponding to the intercept from our power-law extrapolation. This estimated thermal conductivity was found to be $0.16 \pm 0.04 \text{ W K}^{-1} \text{ m}^{-1}$ in good agreement with the experimentally reported values, which are in the range $0.19 - 0.3 \text{ W K}^{-1} \text{ m}^{-1}$.³³⁻³⁵ From figure 3, it can be seen that the irradiated glassy $\text{Ge}_2\text{Sb}_2\text{Te}_5$ models exhibit an increased thermal-relaxation time which ultimately leads to a decreased thermal conductivity. The estimated lattice thermal conductivity of the self-irradiated configurations was found to be in the range of 0.067 to $0.113 \text{ W K}^{-1} \text{ m}^{-1}$, depending on the thermal-spike energy, further revealing that the thermal conductivity could be significantly lowered by controlled irradiation. It is noted that controlled irradiation (with He ions) has been used successfully before to lower the lattice thermal conductivity of Si nanowires.³⁶

In a recent AEMD study for a related glassy chalcogenide material, namely GeTe_4 , the authors reported a value of $0.013 \pm 0.003 \text{ W K}^{-1} \text{ m}^{-1}$ for the thermal conductivity,³⁷ which is an order of magnitude lower than the experimental measurement for this material ($0.1 \text{ W K}^{-1} \text{ m}^{-1}$).³⁸ This discrepancy is likely due to the small model system size (185 atoms), which illustrates the limitations of tractable *ab initio* molecular-dynamics simulations. The same authors, in a different study,³⁹ doubled the simulated system size (up to 370 atoms) and obtained

a value of $0.044 \pm 0.001 \text{ W K}^{-1} \text{ m}^{-1}$ for the thermal conductivity of glassy GeTe_4 , closer to, but still smaller than, the experimental value, revealing the influence of size effects.

The relatively low estimated value for the thermal conductivity of glassy $\text{Ge}_2\text{Sb}_2\text{Te}_5$ in this work could suggest that the system size is still somewhat too small to fully account for the contribution of any long-wavelength vibrational modes to the lattice thermal conductivity.^{8,40} While not a substitute for analysing the finite-size effects, the influence of the boundary region Langevin-thermostat damping time was included in our estimates of the lattice thermal conductivity and is discussed in the Supplemental Material.

In conclusion, a non-equilibrium molecular-dynamics methodology is proposed for calculating the lattice thermal conductivity of a cubic-core region as it approaches equilibrium with a thermostatted-boundary layer. This approach has been applied to estimate the change in the lattice thermal conductivity with thermal-spike energy in self-irradiated glassy $\text{Ge}_2\text{Sb}_2\text{Te}_5$ models. As the irradiated core approached equilibrium with the thermostatted boundary, the thermal relaxation time is fitted using an appropriate time interval from the asymptotic regime of the simulation. The good agreement obtained between the calculated value for the lattice thermal conductivity of pristine glassy $\text{Ge}_2\text{Sb}_2\text{Te}_5$ and the results of experimental measurements provides validation for this approach.

The thermal relaxation time is found to increase as a sublinear power-law function of the thermal-spike energy. This results in an overall decrease of the lattice thermal conductivity compared to that of the pristine glassy structure. Our simulations suggest that radiation-induced cascades can therefore reduce the lattice thermal conductivity of glassy $\text{Ge}_2\text{Sb}_2\text{Te}_5$ by as much as 60%. Given the remarkable recovery of the electronic structure of the glass after irradiation, as already demonstrated for this material in our previous work,²³ ion irradiation can therefore be a potential strategy for improving the performance of phase-change memory and data-storage devices by reducing thermal cross-talk between memory cells. While the qualitative trends should stay the same, in the future, these effects should be explored in larger models which allow for better statistics and a wider range of higher thermal-spike energies, as well as in models of the crystalline phases of $\text{Ge}_2\text{Sb}_2\text{Te}_5$.

See [Supplemental Material](#) for details about the thermal profiles established in the asymptotic regime in the irradiated glass, the calculation of the heat capacity in the simulated systems and the effect of the Langevin-thermostat damping time during irradiation on the calculation of the thermal conductivity.

F.C.M. acknowledges financial support from the UK Engineering and Physical Sciences Research Council (EPSRC) Centre for Doctoral Training in Compu-

tational Methods for Materials Science under grant EP/L015552/1, and resources provided by the “Cambridge Service for Data Driven Discovery” (CSD3, <http://csd3.cam.ac.uk>) system operated by the University of Cambridge Research Computing Service (<http://www.hpc.cam.ac.uk>) and funded by EPSRC Tier-2 capital grant EP/P020259/1. Via our membership of the UK’s HEC Materials Chemistry Consortium, which is funded by EPSRC (EP/L000202, EP/R029431), this work used the ARCHER UK National Supercomputing Service (<http://www.archer.ac.uk>). K.K. acknowledges financial support from the EPSRC grant EP/N022009/1 (“Development and Application of Non-Equilibrium Doping in Amorphous Chalcogenides”), and also acknowledges the use of the High Performance Computing Facility (Grace@UCL), and associated support services, in the completion of this work.

REFERENCES

- ¹M. A. Modestino and S. Haussener, *Annu. Rev. Chem. Biomed. Eng.* **6**, 13 (2015).
- ²M. Zebarjadi, *Sci. Rep.* **6**, 20951 (2016).
- ³S. R. Elliott, *Int. J. Appl. Glass Sci.* **6**, 15 (2015).
- ⁴S. W. Fong, C. M. Neumann, and H. S. Wong, *IEEE Transactions on Electron Devices* **64**, 4374 (2017).
- ⁵D. Lencer, M. Salinga, and M. Wuttig, *Adv. Mater.* **23**, 2030 (2011).
- ⁶G. C. Sosso, D. Donadio, S. Caravati, J. Behler, and M. Bernasconi, *Phys. Rev. B* **86**, 104301 (2012).
- ⁷D. Campi, D. Donadio, G. C. Sosso, J. Behler, and M. Bernasconi, *J. Appl. Phys.* **117**, 015304 (2015).
- ⁸G. C. Sosso, V. L. Deringer, S. R. Elliott, and G. Csányi, *Mol. Sim.* **44**, 866 (2018).
- ⁹D. Campi, L. Paulatto, G. Fugallo, F. Mauri, and M. Bernasconi, *Phys. Rev. B* **95**, 024311 (2017).
- ¹⁰S. Baroni, R. Bertossa, L. Ercole, F. Grasselli, and A. Marcolongo, in *Handbook of Materials Modeling* (Springer International Publishing, Cham, 2018) pp. 1–36, [arXiv:1802.08006](https://arxiv.org/abs/1802.08006).
- ¹¹D. A. Broido, M. Malorny, G. Birner, N. Mingo, and D. A. Stewart, *Appl. Phys. Lett.* **91**, 231922 (2007).
- ¹²J. Carg, N. Bonini, B. Kozinsky, and N. Marzari, *Phys. Rev. Lett.* **106**, 045901 (2011).
- ¹³A. Marcolongo, P. Umari, and S. Baroni, *Nat. Phys.* **12**, 80 (2016).
- ¹⁴C. Carbogno, R. Ramprasad, and M. Scheffler, *Phys. Rev. Lett.* **175901**, 118 (2017).
- ¹⁵E. Lampin, Q. H. Nguyen, P. A. Francioso, and F. Cleri, *Appl. Phys. Lett.* **100**, 131906 (2012).
- ¹⁶E. Lampin, P. L. Palla, P. A. Francioso, and F. Cleri, *J. Appl. Phys.* **114**, 033525 (2013).
- ¹⁷M. Puligheddu, F. Gygi, and G. Galli, *Phys. Rev. Mater.* **1**, 060802 (2017).
- ¹⁸T. H. Lee and S. R. Elliott, *Adv. Mater.* **29**, 1700814 (2017).
- ¹⁹A. Tenenbaum, G. Ciccotti, and R. Gallico, *Phys. Rev. A* **25**, 2778 (1982).
- ²⁰D. Toton, C. D. Lorenz, N. Rompotis, N. Martsinovich, and L. Kantorovich, *J. Phys.: Condens. Matter* **22**, 074205 (2010).
- ²¹J. Vandevondele, M. Krack, F. Mohamed, M. Parrinello, T. Chassaing, and J. Hutter, *Comput. Phys. Commun.* **167**, 103 (2005).
- ²²L. Kantorovich and N. Rompotis, *Phys. Rev. B* **78**, 094305 (2008).
- ²³K. Konstantinou, T. H. Lee, F. C. Mocanu, and S. R. Elliott, *Proc. Natl. Acad. Sci. USA* **115**, 5353 (2018).
- ²⁴K. Konstantinou, F. C. Mocanu, T. H. Lee, and S. R. Elliott, *J. Phys.: Condens. Matter* **30**, 455401 (2018).
- ²⁵P. L. Kapitza, *Physical Review* **60**, 354 (1941).
- ²⁶A. Singh and E. B. Tadmor, *J. Appl. Phys.* **117**, 185101 (2015).
- ²⁷N. A. Marks, *Phys. Rev. B* **56**, 2441 (1997).
- ²⁸J. T. Buchan, M. Robinson, H. J. Christie, D. L. Roach, D. K. Ross, and N. A. Marks, *J. Appl. Phys.* **117**, 245901 (2015).
- ²⁹M. Ceriotti, G. Bussi, and M. Parrinello, *Phys. Rev. Lett.* **102**, 020601 (2008).
- ³⁰M. Ceriotti, G. Bussi, and M. Parrinello, *J. Chem. Theory Comput.* **6**, 1170 (2010).
- ³¹M. Kuwahara, O. Suzuki, Y. Yamakawa, N. Taketoshi, T. Yagi, P. Fons, T. Fukaya, J. Tominaga, and T. Baba, *Jap. J. Appl. Phys.* **46**, 3909 (2007).
- ³²P. Zalden, K. S. Siegert, S. Rols, H. E. Fischer, F. Schlich, T. Hu, and M. Wuttig, *Chem. Mater.* **26**, 2307 (2014).
- ³³C. Peng, L. Cheng, and M. Mansuripur, *J. Appl. Phys.* **82**, 4183 (1997).
- ³⁴V. Giraud, J. Cluzel, V. Sousa, A. Jacquot, A. Dauscher, B. Lenoir, H. Scherrer, and S. Romer, *J. Appl. Phys.* **98**, 13520 (2005).
- ³⁵H. K. Lyee, D. G. Cahill, B. S. Lee, J. R. Abelson, M. H. Kwon, K. B. Kim, S. G. Bishop, and B. K. Cheong, *Appl. Phys. Lett.* **89**, 151904 (2006).
- ³⁶Y. Zhao, D. Liu, J. Chen, L. Zhu, A. Belianinov, O. S. Ovchinnikova, R. R. Unocic, M. J. Burch, S. Kim, H. Hao, D. S. Pickard, B. Li, and J. T. Thong, *Nat. Comm.* **8**, 15919 (2017).
- ³⁷A. Bouzid, H. Zaoui, P. Luca Palla, G. Ori, M. Boero, C. Massobrio, F. Cleri, and E. Lampin, *Phys. Chem. Chem. Phys.* **19**, 9729 (2017).
- ³⁸S. N. Zhang, J. He, T. J. Zhu, X. B. Zhao, and T. M. Tritt, *J. Non-Cryst. Solids* **355**, 79 (2009).
- ³⁹E. Martin, P. L. Palla, F. Cleri, A. Bouzid, G. Ori, S. Le Roux, M. Boero, and C. Massobrio, *J. Non-Cryst. Solids* **498**, 190 (2018).
- ⁴⁰P. B. Allen and J. L. Feldman, *Phys. Rev. B* **48**, 12581 (1993).